SHAPE AND FISSION INSTABILITY OF ROTATING NUCLEI AT FINITE TEMPERATURES

By M. E. Faber*

Institut für Kernphysik der Technischen Universität, Wien, Austria

M. Ploszajczak

Centre de Recherches Nucléaires et Université Louis Pasteur de Strasbourg, Groupe de Physique Nucléaire Théorique, BP 20 67037 Strasbourg-Cedex, France

and

Institute of Nuclear Physics, PL-31-324 Kraków, Poland

and K. Junker**

Swiss Institute for Nuclear Research (SIN), CH-5234 Villigen, Switzerland

(Received March 2, 1984)

A model for the unified treatment of rotations and thermal excitations is proposed, in which the single particle (s.p.) level density $g(\varepsilon)$ is renormalized with respect to the liquid drop (LDM) density $g_{\mathrm{LDM}}(\varepsilon)$. In this way the erroneous behaviour of the smoothed s.p. level density $\tilde{g}(\varepsilon)$ as a function of the deformation of the nucleus is removed. This is particularly important in the range of large deformations as encountered in fissioning nuclei. The model is then applied to nuclei in the actinide region to study their shape and their stability against fission. The structure of the fission barriers of rotating, heated nuclei is studied in detail. The shell corrections to the energy, free energy and angular momentum ase calculated by means of a deformed Saxon-Woods (SW) potential.

PACS numbers: 25.85.-w, 21.60.-n

1. Introduction

Nuclei at extremely high angular momenta can be formed in fusion reactions between heavy ions (HI). During the early stage of the deexcitation process the compound nucleus is cooled either by fission or by emission of light particles, mainly neutrons, protons and

* Postal address: Schüttelstr. 115, A-1020 Wien.

** Permanent address: Swiss Federal Institute for Reactor Research (EIR), CH-5303 Würenlingen, Switzerland.

α-particles. At lower excitation energies close to the entry line, the emission of γ-rays and high-L α-particles [1] becomes the dominant process. Earlier cranking Strutinsky (CS) — and cranking Hartree-Fock-Bogoliubov (CHFB)-calculations [2–7] described the rotating nucleus in the zero temperature limit $T = 0$. This is a good approximation for spins much lower than the initial angular momentum I_i of the compound system. However for angular momenta $I \simeq I_{CRIT}$ close to the oblate-prolate shape instability [8] it is practically impossible to form a cold nucleus in a HI-reaction. Thus, an appropriate estimate of the various competing deexcitation channels as well as the shape stability of the rotating compound nucleus requires the inclusion of thermal excitations.

First calculations of rotating heated nuclei have been performed independently by the Dubna group [9] and by Faber and Ploszajczak [10]. The Dubna group used the Nilsson potential in the β, γ-space only. Therefore, their calculations suffered from the absence of the neck deformation which was shown to be of primary importance at $I > I_{CRIT}$ [7]. Moreover, the Dubna group calculated the excitation energies in the Strutinsky approach as the difference between the energies of the heated system and the system at the yrast line, respectively. It is known [11] that the smoothed s.p. level density $\tilde{g}(\varepsilon)$ of realistic s.p. potentials shows an erroneous dependence on deformation, thus inducing a spurious deformation dependent contribution to the excitation energy of a heated nucleus. This difficulty can be avoided if the smoothed level density is renormalized by a suitable liquid drop level density $g_{LDM}(\varepsilon, T = 0)$ [12] as described in Sects. 2.4 and 3.2.

Recently, another approach for calculating properties of heated, rotating nuclei has been proposed [13]. They introduced a temperature-dependent liquid drop model (TDLDM) [14] with parameters in accord with the Thomas-Fermi model of excited nuclei [15]. The microscopically calculated free energy surface is renormalized with respect to the classical free energy surface of the TDLDM. This renormalization procedure corresponds to the approach proposed in Ref. [10].

It is the aim of this work to investigate the fission and shape instability of nuclei at high excitations. To accomplish this we develop a model based on the Strutinsky approach extended to finite temperatures and angular momenta. The details of our model are discussed in Chapter 2. The model is used to calculate the potential energy and the free energy surfaces in the space $(\beta, r, \gamma, \alpha)$, where β describes the elongation, r the neck formation, γ the axial asymmetry and α the reflection asymmetry.

In Chapter 3 we compare isentropic and isothermal nuclear processes and study the symmetric fission of heated, fast rotating nuclei ^{210}Po and ^{238}U. In Chapter 4 the dependence of the fission barrier height on nonaxial deformation γ and reflection asymmetry α for ^{238}U is discussed. We investigate the existence of two separate fission channels for finite values of I and T. First evidence for the existence of two separate channels for mass symmetric and asymmetric fission came from both experimental [16] and theoretical investigations [17] of fission at low (zero) angular momentum and low (zero) excitation energy.

Finally, in Chapter 5 we summarize main results of this work.

2. Theory

2.1. Parametrization of the nuclear shape

One may introduce the neck- and reflection asymmetry parameters as an extension of the β, γ-parametrization. In cylindrical coordinates (R, z, φ) the axially symmetric "modified spheroids" are defined by [18]:

$$R^2(z) = R_z^2[1-(z/R_z)^2]F(z, R_z), \tag{2.1}$$

where

$$F(z, R_z) = \sum_i [a_{2i}(z/R_z)^{2i} + a_{2i+1}(z/R_z)^{2i+1}]. \tag{2.2}$$

In practical applications one uses only the first few terms:

$$F(z/R_z) \approx a + \alpha(z/R_z) + b(z/R_z)^2. \tag{2.3}$$

Such a function approximates closely the family of thresholds shapes studied by Cohen and Swiatecki [19]. Introducing the dimensionless cylindrical coordinates $u, v, w (u = x/R_z = \varrho \cos\varphi, v = y/R_z = \varrho \sin\varphi, w = z/R_z)$ one can write Eq. (2.1) as follows:

$$\varrho^2 = (1-w^2)(A + \alpha w + Bw^2). \tag{2.4}$$

Instead of the non-illustrative parameters A and B we prefer to keep the ellipsoidal deformation parameters β and γ of Bohr [20] and to introduce an additional parameter r [7] describing the formation of a neck. The parameter r is defined as the ratio of the neck cross section at $w = 0$ and the cross section of the equivalent ellipsoid at the same position $(w = 0)$ (see Fig. 1). The equivalent ellipsoid has the same volume as the deformed nucleus

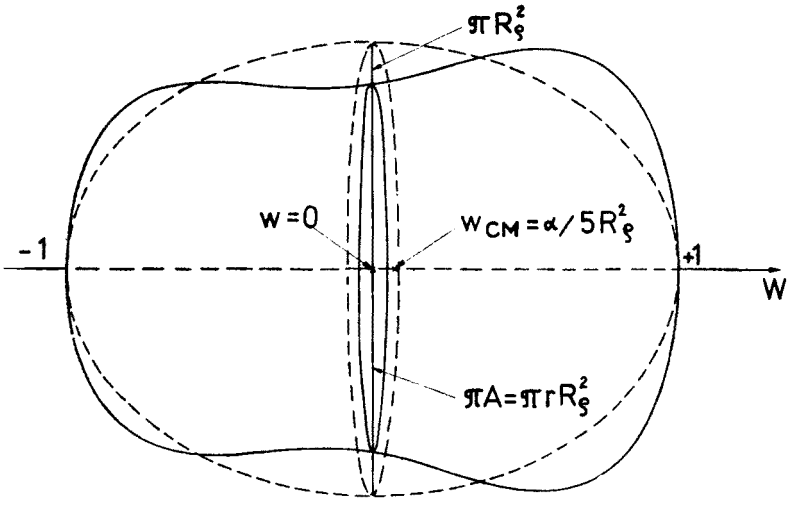

Fig. 1. Schematic picture of the reflection asymmetric dumb-bell shape and the corresponding equivalent ellipsoidal shape

under consideration. The length of the longer axis is kept constant and equals 1. Thus, the ellipsoid is characterized by the equivalent radius

$$R_\varrho(\beta, \gamma) = \sqrt{R_u R_v} = [1+\sqrt{5/4\pi}\,\beta\cos\gamma]^{-1}\{[1+\sqrt{5/4\pi}\,\beta\cos(\gamma-\tfrac{2}{3}\pi)] \times [1+\sqrt{5/4\pi}\,\beta\cos(\gamma-\tfrac{4}{3}\pi)]\}^{1/2}. \tag{2.5}$$

The cross section at $w = 0$ (see Fig. 1) is then:

$$S(w=0) = \pi r R_\varrho^2 = \pi A. \tag{2.6}$$

For $r = 1$ one obtains ellipsoidal shapes, for $r > 1$ diamond-like shapes, whereas neck ratios $0 < r < 1$ ($\alpha = 0$) describe configurations with a neck. The second equation relating the parameters A, B with r and $R_\varrho(\beta, \gamma)$ can be obtained from the volume conservation condition. The odd powers in the "neck function" $F(w)$ change the mean values of u^2 and w^2 as well as the center of gravity w_{CM} which becomes:

$$w_{CM} = \alpha/5R_\varrho^2 \tag{2.7}$$

for a dumb-bell configuration.

2.2. Thermodynamic description of heated, rotating nuclei

A particularly convenient description of the heated nucleus is provided by the grand canonical ensemble. This ensemble is specified by $\psi_{st} = \exp\{-(H_0-\omega J_x-\mu N)/T\}$ or its trace, the grand partition function $Z(T, \omega, \mu) = \mathrm{tr}\,\psi_{st}$.

In the deformed shell model used in this work, Z equals:

$$Z(T, \omega, \mu, \vec{q}) = \prod_i \{1+\exp[-(\varepsilon_i(\omega, \vec{q})-\mu)/T]\}, \tag{2.8}$$

where $\vec{q}$ is the nuclear deformation. (For simplicity, we do not write isospin indices.) Having calculated the grand partition function one easily obtains the total energy R in the rotating system

$$R(T, \omega, \mu, \vec{q}) = \sum_i \varepsilon_i(\omega, \vec{q}) n_i(T, \omega, \mu, \vec{p}), \tag{2.9}$$

where n_i is the occupation probability of a s.p. state, the angular momentum I

$$I(T, \omega, \mu, \vec{q}) = \sum_i \langle j_x\rangle_{ii}(\omega, \vec{q}) n_i(T, \omega, \mu, \vec{q}) \tag{2.10}$$

and the energy in the laboratory system

$$E(T, \omega, \mu, \vec{q}) = R+\omega I = \sum_i [\varepsilon_i(\omega, \vec{q})+\omega\langle j_x\rangle_{ii}] n_i. \tag{2.11}$$

The differential

$$d\Omega = \frac{\partial\Omega}{\partial T}dT + \frac{\partial\Omega}{\partial\omega}d\omega + \frac{\partial\Omega}{\partial\mu}d\mu + \frac{\partial\Omega}{\partial\vec{q}}d\vec{q} = -SdT - Id\omega - Nd\mu - \vec{p}d\vec{q} \tag{2.12}$$

of a thermodynamical potential $\Omega = -T \ln Z$ allows the identification of the entropy S and the generalized force $\vec{p}$ as conjugate quantities to the temperature T and the deformation $\vec{q}$:

$$S = -\partial\Omega/\partial T|_{\mu,\omega,\vec{q}}, \quad \vec{p} = -\partial\Omega/\partial\vec{q}|_{T,\mu,\omega}. \tag{2.13}$$

Analogous differential of the energy and the free energy are

$$dE = TdS + \omega dI + \mu dN - \vec{p}d\vec{q}, \quad dF = -SdT + \omega dI + \mu dN - \vec{p}d\vec{q} \tag{2.14}$$

and the driving force $\vec{p}$ can be expressed as follows:

$$\vec{p} = \partial E/\partial\vec{q}|_{S,I,N} = -\partial F/\partial\vec{q}|_{T,I,N}. \tag{2.15}$$

Thus $\vec{p}$ depends only on the state of the system and not on the particular process leading to this state. Consequently, the energy surface $E(\vec{q})$ for a given $I_1, N_1, T_1[S(\vec{q}) = S(\vec{q}, I_1, N_1, T_1)]$ reminds closely the free energy surface $F(\vec{q})$ for $I_1, N_1, S_1[T(\vec{q}) = T(\vec{q}, I_1, N_1, S_1)]$ providing the mean value of entropy $\bar{S}$ in the state I_1, N_1, T_1 equals S_1 or the mean value of temperature $\bar{T}$ in the state I_1, N_1, S_1 equals T_1. To see this let us consider the difference of F and E around $\bar{S} = S_1$ and T_1 respectively.

$$\int_{\vec{q}_1}^{\vec{q}_2} \left[\left. \frac{\partial F(\vec{q}, T_1)}{\partial \vec{q}} \right|_T - \left. \frac{\partial E(\vec{q}, \bar{S})}{\partial \vec{q}} \right|_S \right] d\vec{q} = \int_{\vec{q}_1}^{\vec{q}_2} \left[\left. \frac{\partial E(\vec{q}, T_1)}{\partial \vec{q}} \right|_{S=\text{const!}} - \left. \frac{\partial E(\vec{q}, \bar{S})}{\partial \vec{q}} \right|_S \right] d\vec{q}$$

$$\simeq -\int_{\vec{q}_1}^{\vec{q}_2} \frac{\partial \vec{p}(\vec{q}, \bar{S})}{\partial S} \delta S(\vec{q}, T_1) d\vec{q}, \tag{2.16}$$

where $\delta S(\vec{q}, T_1) = S(\vec{q}, t_1) - \bar{S}$. This difference is extremely small because both $\delta S(\vec{q}, T_1)$ and $\partial\vec{p}/\partial S$ are small.

The energy variations in isothermal and isentropic processes may differ significantly ($dE|_T = dE|_S + TdS$). For isothermal processes a heat bath is required to supply the thermal energy $dQ = TdS$. In nuclei the source of this additional energy is the collective kinetic energy. If the collective coordinate $\vec{q}$ changes from a minimum towards a saddle point then the entropy increases ($dS > 0$) and the heat dQ is transferred from the collective kinetic energy to the internal excitation energy. Creation of these additional p-h excitations can be achieved either by inelastic collisions between the nucleons or by friction forces. One expects that fusion of two colliding ions is predominantly an isothermal process.

For the opposite deformation change, namely from the saddle to the scission point an isothermal process is impossible. The entropy cannot decrease and heat energy cannot be transformed into energy of collective motion. So one can infer that fission is predominantly an isentropic process.

2.3. Temperature dependent liquid drop model (TDLDM)

Particle-hole (p–h) excitations in heated nuclei lead to a change in the occupancy of s.p. orbitals around the Fermi level. Nucleons are excited from occupied levels below the Fermi surface into higher shells. This induces changes in the average potential decreasing the depth and increasing the surface thickness of the potential. In the framework of the Strutinsky model these variations can be taken into account by introducing a temperature dependence into the liquid drop energy [13–15, 21].

Sauer and Chandra [21] have studied the thermal properties of infinite nuclear matter in the Hartree-Fock (HF) approximation using a Skyrme force. In this approximation, the temperature dependence of the nucleon density n and the nuclear radius R are given by:

$$n(T) = n(0)\,[1-\alpha_n T^2], \tag{2.17}$$

$$R(T) = R(0)\,[1+\alpha_R T^2], \tag{2.18}$$

where $\alpha_n = 1.23 \cdot 10^{-3}\ \mathrm{MeV}^{-2}$, $\alpha_R = 4.2 \cdot 10^{-4}\ \mathrm{MeV}^{-2}$. The temperature T is given in units of MeV. This density variation induces a change of the volume term in the liquid drop binding energy:

$$E_v(T) = E_v(0)\,[1-\alpha_v T^2], \quad \alpha_v = \alpha_n. \tag{2.19}$$

In Ref. [21], the volume energy contains contributions from statistical p-h-excitations. Consequently, the temperature variations of E_v are almost three times smaller ($\alpha_v = 3.4 \cdot 10^{-4}\ \mathrm{MeV}^{-2}$) as compared to Eq. (2.19). Since we determine the energy of p-h excitations directly from the s.p. spectrum, therefore, it is sufficient to include the temperature variations of E_v only through its dependence on $n(T)$ (Eq. (2.29)).

Three effects contribute to a change of the surface energy E_s with temperature: the decrease of the nucleon density, the increase of the nuclear surface and the increase of the surface thickness. For a constant nuclear radius, E_s is proportional to the nucleon density and becomes zero in the limit of vanishing nucleon density. Consequently, the change of E_s caused by variations of n is $-E_s(0)\alpha_v T^2$. An increase of the nuclear surface increases the surface energy by $E_s(0)\,\dfrac{2\alpha_v}{3}\,T^2$. Thus, these two contributions cancel to a large extent. The contribution coming from increasing surface thickness $a(T)$ has been eliminated in the HF-approximation with Skyrme forces [21]. Using this result we obtain:

$$a(T) = a(0)\,[1+\alpha_a T^2], \tag{2.20}$$

$$E_s(T) = E_s(0)\,[1+\alpha_s T^2], \tag{2.21}$$

where $\alpha_a = 8.10^{-3}\ \mathrm{MeV}^{-2}$ and $\alpha_s = 9.10^{-3}\ \mathrm{MeV}^{-2}$.

The Coulomb energy E_c decreases with increasing temperature due to the increase of both the nuclear radius and the surface thickness. The change of E_c caused by the temperature dependence of R is equal to $-E_c(0)\,(\alpha_v/3)T^2$. Its dependence on the surface thick-

ness is given by [22]

$$E_c(a) = E_c(a=0)\left[1-\tfrac{5}{2}\left(\frac{a}{R}\right)^2\right] \tag{2.22}$$

and therefore the change of E_c is equal to $-E_c(0)5[a(0)/R(0)]^2(\alpha_s+\alpha_v/3)T^2$. Thus, the temperature dependence of the Coulomb energy is

$$E_c(T) = E_c(0)\{1-[\alpha_v/3+5(a(0)/R(0))^2(\alpha_s+\alpha_v/3)]T^2\}. \tag{2.23}$$

From the HF studies of Ref. [16] one can estimate the change of the volume asymmetry energy E_t with temperature:

$$E_t(T) = E_t(0)[1+\alpha_t T^2](N-Z)^2/A, \quad \alpha_t = 2.10^{-4}\ \mathrm{MeV}^2. \tag{2.24}$$

To complete the study of TDLDM let us consider variations of the moment of inertia θ with temperature. In the rotating liquid drop model (RLDM) θ is determined by integrating over a uniform mass distribution inside the nuclear surface. Such a geometrical moment of inertia $\theta_{\mathrm{geom}}(T, \vec{q})$ increase with temperature due to the increase of both the nuclear radius and the surface diffuseness:

$$\theta_{\mathrm{geom}}(T, \vec{q}) = \theta_{\mathrm{geom}}(0, \vec{q})\left[1+\left(\tfrac{2}{3}\alpha_v+\tfrac{40}{3}\frac{a^2}{R^2}\alpha_s\right)T^2\right]. \tag{2.25}$$

In heavy nuclei a change of temperature from $T = 0$ to $T = 1$ MeV (3 MeV) leads to an increase of θ_{geom} of roughly 2‰ (2%). In the LDM the temperature dependence of the

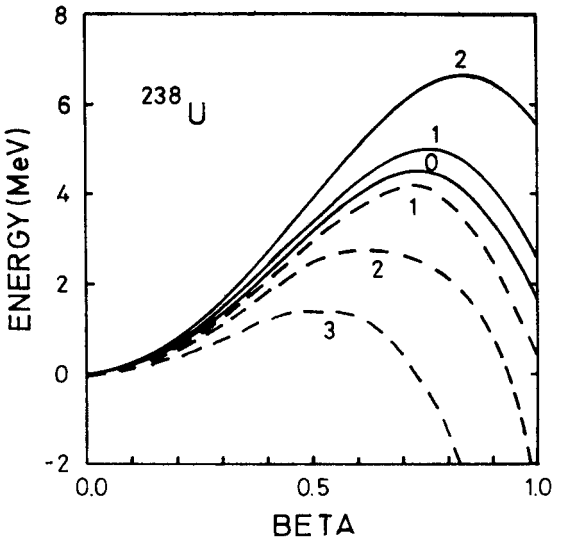

Fig. 2. The liquid drop fission barrier of ^{238}U along the liquid drop valley for isothermal (full lines) and isentropic (dashed lines) processes

free energy F can easily be determined from Eq. (2.14) after solving a linear differential equation

$$S = -\partial F/\partial T|_{\vec{q}} \tag{2.26}$$

with the initial condition $F(T=0) = E(T=0)$. Assuming a quadratic dependence of the LD-energy on T, one obtains

$$F_{\mathrm{LDM}}(T) = E_{\mathrm{LDM}}(0)\,[1-\alpha T^2], \quad S_{\mathrm{LDM}}(T) = 2T\alpha E_{\mathrm{LDM}}(0), \tag{2.27}$$

where

$$\alpha = \{-\alpha_v E_v(0)+(\alpha_s-\alpha_v/3)E_s(0)-[\alpha_v/3+5(a_0/R_0)^2(\alpha_s+\alpha_v/3)]E_c(0)+\alpha_t E_t(0)\}/E_{\mathrm{LDM}}(0). \tag{2.28}$$

It is interesting to study the influence of temperature on the height of the fission barrier in the isothermal ($E(\vec{q})|_T$) limit. Fig. 2 shows isothermal (solid lines) and isentropic. (dashed lines) LD-fission barriers of ^{238}U. These curves have been obtained along the fission valley by solving Eqs. (2.26–2.28). The isothermal barrier increases with T. The saddle point moves towards larger elongations and smaller neck cross sections. On the contrary, the isentropic barrier decreases with T and the corresponding saddle point move towards the spherical shape. These qualitative features of isothermal and isentropic fission barriers are quite general and can be deduced directly from Eqs. (2.26–2.28).

2.4. Strutinsky shell correction approach for heated nuclei

The Strutinsky shell correction method was originally proposed to calculate the deformation energy at $T = 0$. It has been suggested in Refs. [9] and [23] that a determination of the behavior of heated nuclei requires a Strutinsky renormalization for $T = 0$ only. However, such a procedure leads to serious errors at large deformations β and small neck ratios r as can be seen in the lower two diagrams of Fig. 7. These errors are due to the spurious deformation dependence of the smoothed s.p. level density $\tilde{g}$ at the Fermi surface for realistic s.p. potentials [11]. This error is then also present in the calculated excitation energy. Consequently, the thermal excitation energy ($E(T, \omega = 0, \vec{q})-E_{\mathrm{RLDM}}(\omega = 0, \vec{q})$ or $E(S, \omega = 0, \vec{q})-E_{\mathrm{RLDM}}(\omega = 0, \vec{q})$] shows a deformation dependence even if shell effects vanish. This problem can be avoided if a smoothed s.p. level density $\tilde{g}(\varepsilon)$ is replaced by a LDM density $g_{\mathrm{LDM}}(\varepsilon)$. This procedure is equivalent to the replacement of the smooth part of the thermodynamical potential by a phenomenological function:

$$\Omega_{\mathrm{LDM}}(\omega) = -T\int_0^\infty g_{\mathrm{LDM}}(\varepsilon)\ln\{1+\exp[(\mu-\varepsilon)/T]\}d\varepsilon, \tag{2.29}$$

where $g_{\mathrm{LDM}}(\varepsilon)$ is constrained by the conditions

$$N = \int_0^\mu g_{\mathrm{LDM}}(\varepsilon)d\varepsilon, \quad E_{\mathrm{LDM}} = \int_0^\mu \varepsilon g_{\mathrm{LDM}}(\varepsilon)d\varepsilon \tag{2.30}$$

and μ is the chemical potential. Unfortunately, the functional form of $g_{\mathrm{LDM}}(\varepsilon)$ cannot be defined uniquely [12, 14]. Here, we use a formula which was derived for the Fermi gas

enclosed in a finite volume [24]. Adding a Coulomb contribution to the density function one obtains [12]

$$g_{\mathrm{LDM}}(\varepsilon) = x_v \sqrt{\varepsilon} - x_s - x_c/\sqrt{\varepsilon}. \tag{2.31}$$

The deformation dependent parameters $x_s(\vec{q})$, $x_c(\vec{q})$ and the parameter x_v are adjusted for each nucleus. As subsidiary conditions one requires a consistency between $g_{\mathrm{LDM}}(\varepsilon)$ and the droplet formula [25] for the depth of a potential as well as an agreement between calculated and experimental nucleon separation energies. In addition, the deformation dependence of the liquid drop binding energy $E_{\mathrm{LDM}}(\vec{q})$ must be reproduced exactly. This can be achieved by the following iterative procedure.

One begins by choosing x_v for which volume energy E_v is calculated

$$\int_0^{\mu''} x_v \sqrt{\varepsilon}\, \varepsilon d\varepsilon = E_v, \tag{2.32}$$

μ'' follows from the particle number conservation

$$\int_0^{\mu''} x_v \sqrt{\varepsilon}\, d\varepsilon = N. \tag{2.33}$$

Then, for a given x_v one determines $x_s(\vec{q})$ by

$$\int_{\varepsilon_0'}^{\mu'} [x_v \sqrt{\varepsilon} - x_s(\vec{q})]\varepsilon d\varepsilon = E_v + E_s(\vec{q}), \tag{2.34}$$

where μ' is given by

$$\int_{\varepsilon_0'}^{\mu'} [x_v \sqrt{\varepsilon} - x_s(\vec{q})] d\varepsilon = N \tag{2.35}$$

and $x_c(\vec{q})$ by

$$\int_{\varepsilon_0}^{\mu} [x_v \sqrt{\varepsilon} - x_s(\vec{q}) - x_c(\vec{q})/\sqrt{\varepsilon}]\varepsilon d\varepsilon = E_v + E_s(\vec{q}) + E_c(\vec{q}), \tag{2.36}$$

$$\int_{\varepsilon_0}^{\mu} [x_v \sqrt{\varepsilon} - x_s(\vec{q}) - x_c(\vec{q})/\sqrt{\varepsilon}] d\varepsilon = N. \tag{2.37}$$

In the above expression $E_s(\vec{q})$ and $E_c(\vec{q})$ denote the surface and Coulomb energies of the LDM. The integrations are performed only over the physically significant, positive values of the density. After determining $x_s(\vec{q})$, $x_c(\vec{q})$ and $\mu(\vec{q})$ the sum of separation energies for protons and neutrons is calculated for the ground state deformation $\vec{q}_0$ and compared with the experimental value $S_p^{(\mathrm{exp})} + S_n^{(\mathrm{exp})}$. This iterative procedure is repeated until a correct value of x_v for the ground state is obtained. For other deformation x_v is kept nearly constant by fixing the level density at the Fermi energy. Therefore Eqs. (2.32–2.37) have to be solved iteratively. In Table I the results for ^{240}Pu are given. The values of $x_s(\vec{q})$ and $x_c(\vec{q})$ are almost the same as the deformation dependent factors $B_s(\vec{q})$ and $B_c(\vec{q})$ of the

TABLE I

The parameters x_v, x_s and x_c of the LDM-density g_{LDM}, the LD-chemical potentials $\mu^{(p)}_{\mathrm{LDM}}$ ($\mu^{(n)}_{\mathrm{LDM}}$) for protons (neutrons) and values of the liquid drop deformation energy E_{LDM} for ^{240}Pu. E_{LDM} is defined with respect to the energy of the cold, nonrotating, spherical liquid drop. Deformation changes of the coefficients x_s and x_c follow the corresponding variations of the liquid drop shape factors $B_s(\vec{q})$ and $B_c(\vec{q})$

(β, r)	x_v	x_s	x_c	B_s	B_c	$\mu^{(p)}_{\mathrm{LDM}}$	$\mu^{(n)}_{\mathrm{LDM}}$	$g^{(p)}_{\mathrm{LDM}}(\mu^{(p)}_{\mathrm{LDM}})$	$g^{(n)}_{\mathrm{LDM}}(\mu^{(n)}_{\mathrm{LDM}})$	E_{LDM}
0.0, 1.0	1.220	0.725	2.918	1.0	1.0	31.1	39.7	5.55	6.50	0.00
0.3, 1.0	1.220	0.733	2.894	1.013	0.993	31.1	39.7	5.55	6.50	1.39
0.6, 1.0	1.224	0.758	2.838	1.046	0.975	31.1	39.7	5.55	6 50	4.30
0.9, 1.0	1.228	0.794	2.746	1.097	0.947	31.0	39.7	5.55	6.50	7.98

surface and Coulomb energies. One can further simplify the calculations introducing a deformation dependent scaling function $s_q(\varepsilon)$:

$$\tilde{g}[s_q(\varepsilon_i)] = g_{\mathrm{LDM}}(\varepsilon, \vec{q}). \tag{2.38}$$

The Strutinsky renormalization for heated nuclei is then obvious, since the smoothed energy for scaled s.p. levels e_i:

$$e_i(\vec{q}) = s_q[\varepsilon_i(\vec{q})] \tag{2.39}$$

and the LD-energy cancel exactly. Therefore, all equations of Section 2.2. can be used without further renormalization.

For the SW potential, the smoothed rotational energy $\frac{1}{2}\omega I$ is approximately equal to the rigid body rotational energy $\frac{1}{2}\omega I_{\mathrm{RLDM}} = \omega^2/(2\theta_{\mathrm{geom}})$. Therefore, $\tilde{g}_\omega(e) = \tilde{g}_{\omega=0}(e) = g_{\mathrm{LDM}}(e)$ and the same scaling function $s_q(\varepsilon)$ can be used for all ω. In principle the temperature dependence of the LD-energy could be hidden in the parameters x_v, x_s and x_c of $g_{\mathrm{LDM}}(\varepsilon)$. However, the relative changes of the level density at the Fermi surface are negligible for $T \lesssim 5$ MeV. Hence, we use the temperature independent parameters x_v, x_s and x_c and add the temperature dependent contributions to the LD-energy in the total energy expression:

$$E_R(T, \omega, \vec{q}) = \sum_i [e_i(\omega, \vec{q}) + \omega\langle j_x\rangle_{ii}] n_i(T, \omega, \vec{q}) + \alpha(\vec{q}) E_{\mathrm{RLDM}}(0, 0, \vec{q}) T^2$$

$$+ [E_{\mathrm{RLDM}}(0, 0, \vec{q}_{\mathrm{sph}}) - \sum_i^N e_i(0, \vec{q}_{\mathrm{sph}})] \tag{2.40}$$

where $n_i(T, \omega, \vec{q})$ is calculated for the scaled s.p. energies e_i. The first term in $E_R(T, \omega, \vec{q})$ includes thermal, rotation and deformation energies as well as the corresponding temperature dependent shell effects. The second term accounts for the temperature variations of both the radius and the diffuseness of the average potential. The third term is a constant and has no physical significance. Other renormalized quantities like the angular momentum I_R (2.10), the entropy S_R (2.13) and the free energy $F_R \equiv E_R - TS_R$ are constructed

TABLE II

A comparison of the renormalized E_R^* and unrenormalized E^* thermal excitation energies calculated for the strongly deformed ($\beta = 0.8$, $r = 0.8$) configuration of ^{240}Pu for various temperatures. a_R and a are the effective level density parameters corresponding to E_R^* and E^*

T [MeV]	0.2	0.4	0.6	0.8	1.0	1.2	1.5	1.8	2.0	2.5	3.0
E_R^* [MeV]	1.779	5.521	11.24	19.28	29.41	41.69	64.15	91.62	112.77	175.79	253.13
a_R	44.48	34.51	31.23	30.12	29.41	28.95	28.51	28.28	28.19	28.13	28.13
E^* [MeV]	1.476	4.217	8.397	14.22	21.64	30.57	46.96	67.11	82.69	129.26	186.39
a	36.90	26.36	23.32	22.23	21.64	21.23	20.87	20.71	20.67	20.68	20.71

similarly as $E_R(T, \omega, \vec{q})$. In Table II the unrenormalized excitation energy $E^* = E(T, \omega = 0, \vec{q}) - E(0, \omega = 0, \vec{q})$ is compared with the renormalized one $E_R^* = E_R(T, \omega = 0, \vec{q}) - E(0, \omega = 0, \vec{q})$ for the nucleus ^{240}Pu at various temperatures and at a deformation close to the second saddle ($\beta = 0.8$, $r = 0.8$). The effective level density parameters given in Table II are defined as $a = E^*/T^2$. These parameters converge to the largely different limits $a_R \sim A/8.5$ and $a \sim A/11.5$ due to the different bulk properties of $\tilde{g}_R(\varepsilon) = \tilde{g}_{LDM}(\varepsilon)$ and $g(\varepsilon)$.

3. *Symmetric fission of heated fast rotating nuclei*

In this work we will restrict the discussion of the various properties of rotating heated nuclei to exemplary nuclei ^{210}Po and ^{238}U. The s.p. energies ε_i and expectation values of the angular momentum compenent j_x are calculated in a deformed SW potential parametrized in terms of quadrupole deformations β and γ, the neck parameter r and the asymmetry parameter α. The Hamiltonian in the rotating frame is given as the sum of the kinetic energy operator t, the cranking term $-\omega j_x$, the central potential V_c, the spin-orbit potential V_{so} and the Coulomb potential V_{Coul}, approximated by a uniformly charged drop with $Z-1$ protons. The eigenfunctions of this Hamiltonian are expanded in a three dimensional harmonic oscillator basis [7]. The eigenstates can be classified using the q-parity $q = (-1)^{n_x} \Sigma_x$. The π-parity is a good quantum number only for reflection symmetric potentials $V(x, y, -z) = V(x, y, z)$. The time reversal symmetry of the Hamiltonian leads for non-rotating potentials to a degeneracy of levels with opposite sign of the q-parity. This degeneracy is removed by the cranking term. Analytical expressions for the matrix elements of t, V_c, V_{so} and j_x are given in Ref. [7]. As basis states we have included only those states which fulfill the condition:

$$E_{def}(n_x, n_y, n_z) = (n_x + \tfrac{1}{2})\hbar\omega_x + (n_y + \tfrac{1}{2})\hbar\omega_y + (n_z + \tfrac{1}{2})\hbar\omega_z \leqslant (N_0 + \tfrac{3}{2})\hbar\omega_0,$$

$$N_0 = 10. \tag{2.41}$$

The parameters of the SW average field are the same as given in Table 2 of Ref. [7]. Pairing correlations have always been neglected.

Actinide nuclei in their equilibrium configuration at high spins show a weak tendency towards triaxial shapes. Thus the spherical or prolate ground state configuration is relatively stable up to the critical angular momentum I_{CRIT}, where the equilibrium shape changes rapidly and the lowest energy minimum corresponds to strongly elongated configurations ($\beta > 0, \gamma \sim 0°$). This justifies the omission of γ-deformations at high spins. For rotating nuclei close to the fission limit, it is more important to include the neck parameter r than the γ-deformation. Therefore, in most of the calculations discussed in Sects. 3–5 we restrict the shape variations to axially and reflection symmetric ($\alpha = 0$, $\gamma = 0°$) configurations in the β, r-plane.

3.1. Rotating nuclei at $T = 0$

The nucleus ^{238}U belongs to the deformed actinide nuclei at the β-stability line. Its deformation energy surface (DES) for various angular momenta at $T = 0$ is shown in Fig. 3. The characteristic feature of these energy diagrams is the "valley structure" which displays the strong coupling of the elongation β and the neck parameter r. This coupling results from the approximate conservation of the shell closures for shape deformations that leave the ratio of the potential axes unchanged. A simultaneous increase (decrease) of the β, r parameters leaves the ratio of axes approximately constant and thus preserves the shell closures. The classical rotation tends to fill the neck. Since the deformation β

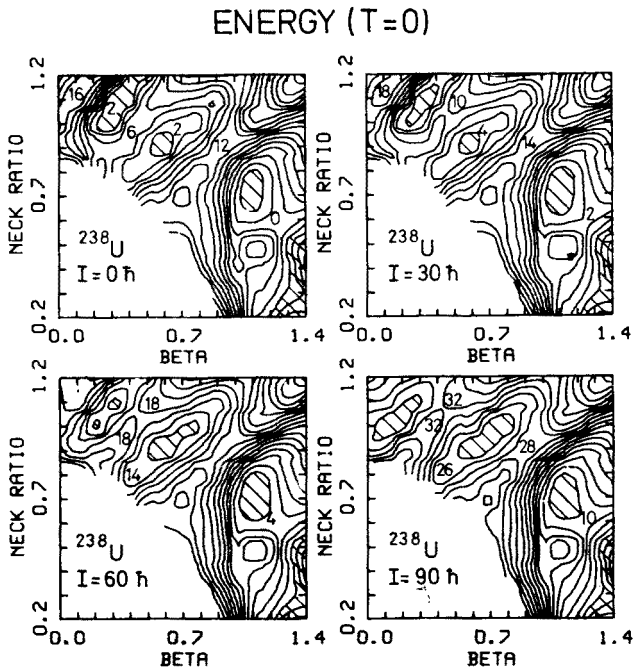

Fig. 3. Deformation energy surfaces at $T = 0$ obtained using the SW-potential and the cranked Strutinsky approach. The energy of ^{238}U is calculated in the $\beta - r$ ($\alpha = 0, \gamma = 0°$) plane for angular momenta $I = 0$, 30, 60 and 90$\hbar$. The dashed areas indicate local minima. The equienergy lines are spaced by 2 MeV and are labelled relative to the energy of the spherical liquid drop at $I = 0$

and r are strongly coupled along the valley, the filling of the neck initiates changes of β. At the ground state valley the decrease of r leads to a shrinking of the nucleus. At the second valley the increase of r results in a stretching of the nucleus. Consequently, the difference of the quadrupole deformations of both minima increases. At $I = 0$ this difference is $\Delta\beta \sim 0.25$ and increases further to $\Delta\beta \sim 0.60$ at $I = 90\hbar$. The filling of the neck by the rotation also changes the shape of the fission valley in the β, r-plane. At $I = 0$ this valley connects the diamond-like shapes at the first minimum, the spheroidal shapes at the first saddle and the dumb-bell shapes at the second minimum and the second saddle. However, at $I = 90\hbar$ the first and the second minimum as well as the first saddle correspond to ellipsoidal shapes and the fission valley begins to tilt towards the dumb-bell configurations around the second saddle.

3.2. Isentropic and isothermal process

Figure 4 shows for ^{238}U the RLD-energy surface at $T = 0$ as well as the free energy surfaces at $T = 1$, 1.5 and 2 MeV. At $I = 60\hbar$ the RLD-energy no longer prevents the nucleus from fission. Therefore, the minimum of the potential energy ($T = 0$) at $\beta \sim 0.55$, $r \sim 0.9$ (see Fig. 3) is stabilized solely by shell effects. The thermal excitations destroy the shell effects and the isothermal fission barrier disappears completely at $T \sim 2$ MeV. According to the TDLDM the height of the fission barrier for isothermal processes increases with temperature (see Fig. 2). This increase is small for temperatures $T \lesssim 1$ MeV and be-

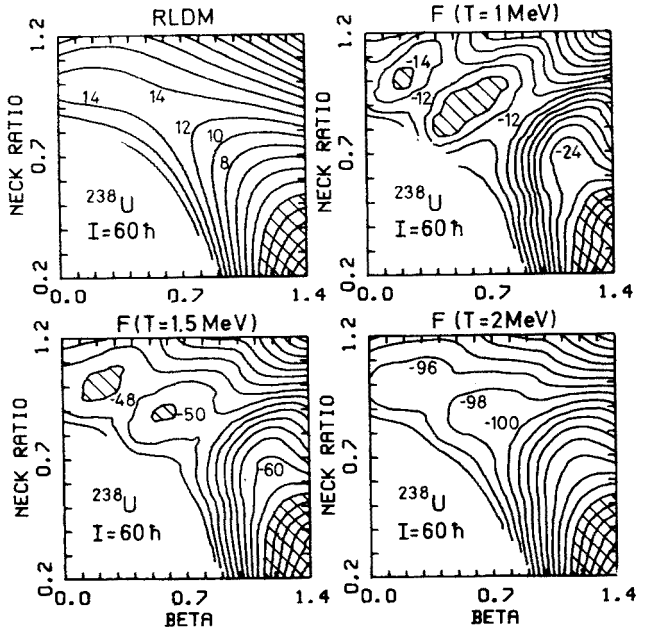

Fig. 4. Various energy surfaces of ^{238}U at $I = 60\hbar$ for axially-and reflection symmetric shapes in the $\beta-r$ plane. The left upper diagram shows the rotating liquid drop energy surface. The right upper and the lower figures present the free energy surfaces at temperatures T of 1, 1.5, 2 MeV, respectively, obtained for the renormalized shell model density $\tilde{g}(\varepsilon)$. The equienergy lines are drawn in steps of 2 MeV and are labelled relative to the energy of the spherical liquid drop at $I = 0$. The dashed areas depict local minima

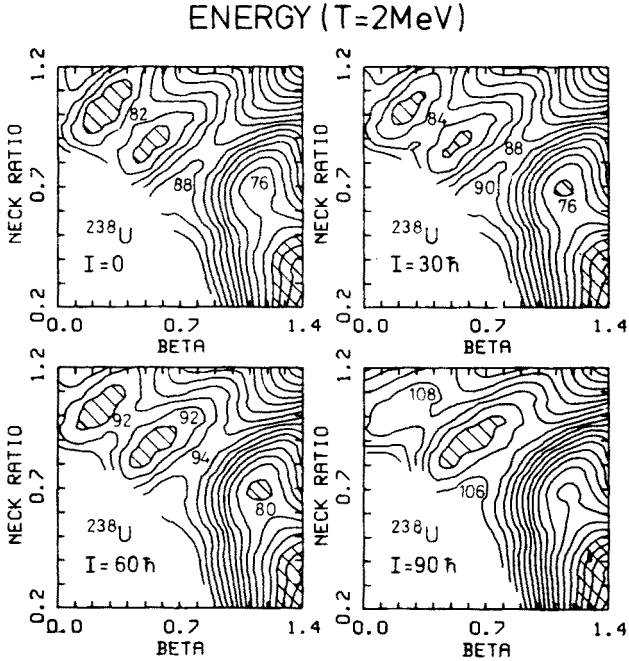

Fig. 5. Isothermal energy surfaces of ^{238}U at $T = 2$ MeV and $I = 0$, 30, 60 and 90$\hbar$. For more details see the caption of Fig. 4

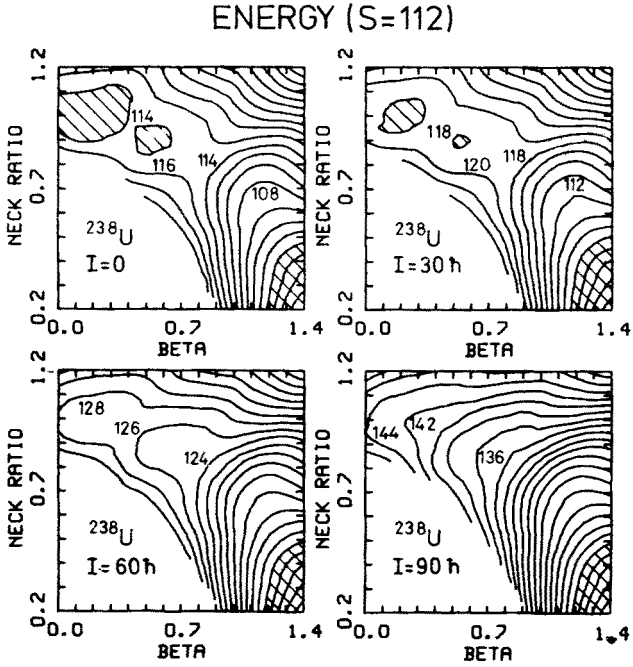

Fig. 6. Isentropic energy surfaces of ^{238}U at $S = 112$ and $I = 0$, 30, 60 and 90$\hbar$. The entropy $S = 112$ corresponds to an average temperature of 2 MeV. For a detailed description see the caption of Fig. 4

comes more and more important for higher temperatures since E_{LDM} depends quadratically on T.

Up to temperature $T \lesssim 3$ MeV the smooth behavior of the energy in the LDM is modified by the shell structure. The variation of isothermal DES's with angular momentum and temperature can be studied in Figs. 3, 5. At $T = 2$ MeV both first and second energy barriers exist up to $I \gtrsim 100\hbar$, whereas in isentropic processes at comparable excitation energies the fission stability is mainly determined by the LDM (compare Fig. 6).

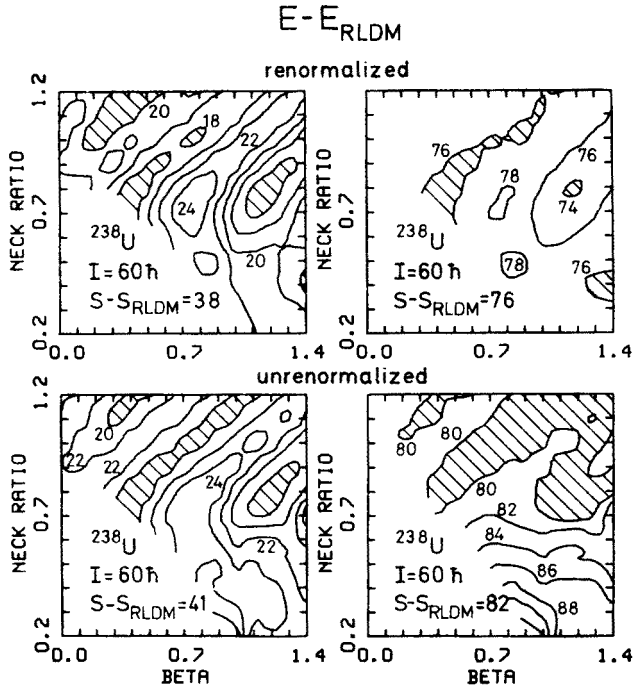

Fig. 7. The sum of the shell energy and the thermal p–h excitation energy for ^{238}U at $I = 60\hbar$. The upper two diagrams are calculated using the renormalized smoothed density of s.p. states $\tilde{g}(\varepsilon)$. In the left diagrams the entropy values $S - S_{\mathrm{RLDM}}$ correspond to an average temperature of 1 MeV, in the right two diagrams to 2 MeV. For further details see the caption of Fig. 4

The energy surface for a constant entropy agrees up to a constant with the respective free energy surface for a constant temperature. This has been discussed in Sect. 2.2 and can be seen by comparing the lower right diagram in Fig. 5 and the lower left diagram in Fig. 6 ($S = 112 \Leftrightarrow \bar{T} = 2$ MeV).

A sizeable flattening of the energy surfaces occurs around minima and saddle points when going from $S = 0$ (Fig. 3) to $S = 112$ ($\Leftrightarrow \bar{T} = 2$ MeV) (Fig. 6). For $S = 0$ the first and second barriers exist at $I > 90\hbar$, whereas for $S = 112$ they disappear already at $I > 60\hbar$. In Fig. 6 one can further study the dependence of the LD-barrier on the excitation energy. The height of the barrier equals ~ 4.5 MeV for $T = 0$, $I = 0$ and becomes $\lesssim 2.5$ MeV at $S = 112$. (The shell structure at $S = 112$ gives only a slight modification of the liquid drop behavior.)

The disappearance of the shell effects at high thermal excitation energies is demonstrated in Fig. 7, where the sum of the shell energy and the thermal p-h excitation energy $\delta E_{\mathrm{sh+th}} = E - E_{\mathrm{RLDM}}$ is shown for isentropic processes of the rotating ($I = 60\hbar$) nucleus ^{238}U. The entropy $S - S_{\mathrm{RLDM}} = 38$ in the upper left diagram corresponds to an average value of the temperature $\bar{T} = 1$ MeV. Similarly, $S - S_{\mathrm{RLDM}} = 76$ in the upper right diagram corresponds to $\bar{T} = 2$ MeV. The lower part of Fig. 7 shows the unrenormalized energies $\delta E^{\mathrm{u.r.}}_{\mathrm{sh+th}}$ [9, 23] for $\bar{T} = 1$ and 2 MeV. In our approach the renormalized shell corrections $\delta E_{\mathrm{sh+th}}$ tend towards a deformation independent constant, whereas the unrenormalized values $\delta E^{\mathrm{u.r.}}_{\mathrm{sh+th}}$ show already at $\bar{T} = 2$ MeV a large unphysical deformation dependence at large elongation and small neck cross section. Thus, the estimate of the excitation energy dependence of the level density parameter for fission a_f and particle emission $a_n(a_p)$ is not meaningful for unrenormalized smoothed level densities $\tilde{g}(\varepsilon)$.

4. The angular momentum and temperature dependence of the fission barrier

This section is devoted to studies of the fission barrier and its structure in ^{210}Po and ^{238}U at high angular momenta and thermal excitations. We determine the fission barriers from the energy surfaces at a constant entropy or equivalently from the free energy surfaces for a constant temperature. To study the I- and T-dependence of the fission barrier we have chosen the spherical nucleus ^{210}Po with two protons outside a double magic ^{208}Pb-core. This nucleus is unstable and it belongs to the neutron-rich side of the β-stability line. The free energy surfaces are minimized in the space of the deformation parameters β and r for $\gamma = 0°$. This is certainly a simplification since nonaxial deformations are important at the first saddle, whereas both the nonaxial and reflection asymmetric deformations play an important role at the second saddle. Both parameters will be included in the detailed investigation of the structure of the fission barrier. At $T = 0$ and finite angular momenta the fission barriers of ^{210}Po were studied in Ref. [7] (see Fig. 15 of Ref. [7]). In this work we present details about barriers at $T > 0$ which are obtained from the free energy surfaces at $T = 0.5$, 1.0, 1.5 and 2 MeV.

Fig. 8 shows the first barrier ($F_A - F_{\mathrm{I}}$), the second barrier ($F_B - F_{\mathrm{II}}$) as well as the energy difference between the first and second energy minima ($|F_{\mathrm{II}} - F_{\mathrm{I}}|$) for ^{210}Po at various temperatures and angular momenta. The heights of both barriers ($F_A - F_{\mathrm{I}}$, $F_B - F_{\mathrm{II}}$) decrease smoothly with increasing temperature due to the destructive influence of temperature on shell effects. For $T < 2$ MeV first barrier disappears at $I \sim 80\hbar$ independent of the thermal excitation energy. The critical spin corresponding to the vanishing second barrier decreases from $I \gtrsim 160\hbar$ at $T = 0$ to $I \sim 110\hbar$ at $T = 1.5$ MeV. At $T = 2$ MeV the shell effects are already too weak to generate a second minimum. Consequently, the fission barrier nearly coincides with the LD-barrier and has to be compared with $F_B - F_{\mathrm{I}}$ at lower temperatures. The critical angular momentum I_{CRIT} for the shape transition from the first to the second minimum ($|F_{\mathrm{I}} - F_{\mathrm{II}}| = 0$) increases slightly with temperature. Moreover, the energy difference $|F_{\mathrm{II}} - F_{\mathrm{I}}|$ at $I > I_{\mathrm{CRIT}}$ increases slowlier at higher temperatures than at low temperatures.

Generally, the shell effects shift up the limiting angular momentum corresponding

to the vanishing fission barrier. The thermal excitations dissolve shell effects and bring the results of the RLDM at $T = 0$ and the CS-approach at $T > 0$ closer to each other. At temperatures higher than $T \sim 1.5$ MeV both models predict similar heights of the fission barrier although the equilibrium deformation and entropy still reflect the presence of the shell structure.

Below, we will also show that the mass distribution of fission fragments may indicate the presence of shell effects even at $T \gtrsim 1$ MeV. Thus, the remnants of shell effects at high

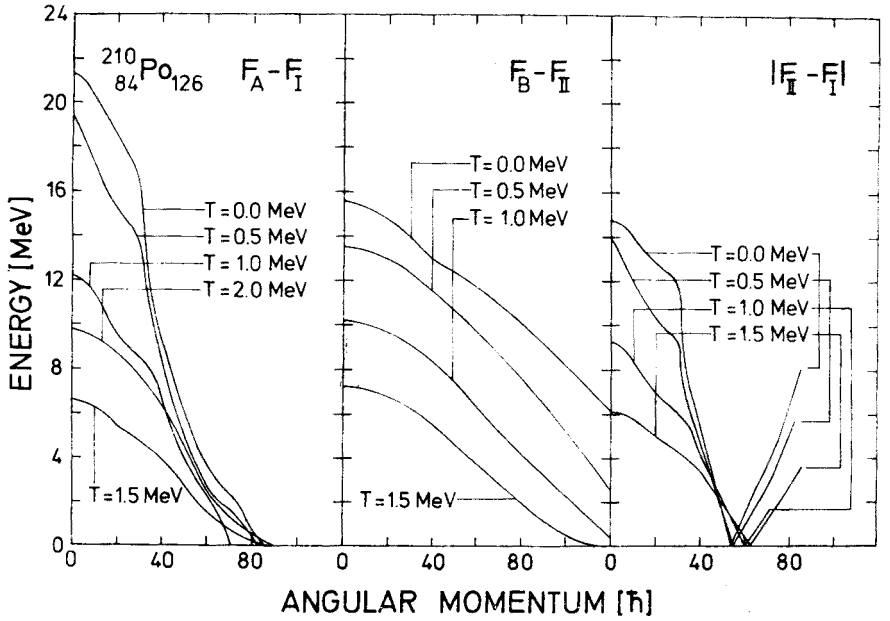

Fig. 8. The first barrier ($F_A - F_I$), the second barrier ($F_B - F_{II}$) and the energy difference between the first and the second free energy minima ($|F_{II} - F_I|$) are plotted as a function of the total angular momentum for various temperatures in ^{210}Po

excitation energies can still be seen in the competition between particle emission and fission for various angular momenta [1].

The mass distribution of the fission products at $I = 0$ in the actinide region often shows a sizeable asymmetry resulting from the reflection asymmetry of the nuclear potential in the region of the fission barrier. The observation of a triple-humped mass distribution by Jensen and Fairhall [26] in ^{226}Ra suggested that the structure of the fission barrier might be even more complicated allowing for the coexistence of mass symmetric and mass asymmetric fission channels. This would indicate also that in certain nuclei one has two separate minima at the fission barrier which correspond to reflection symmetric and reflection asymmetric shapes, respectively. Konecny and Schmitt showed that the ratio of symmetric to asymmetric fission increases with the thermal excitation energy and that symmetric fission becomes dominating at $E^* \geqslant 11$ MeV [27] ($T \gtrsim 0.65$ MeV). The final argument for the coexistence of both the reflection symmetric and asymmetric shapes

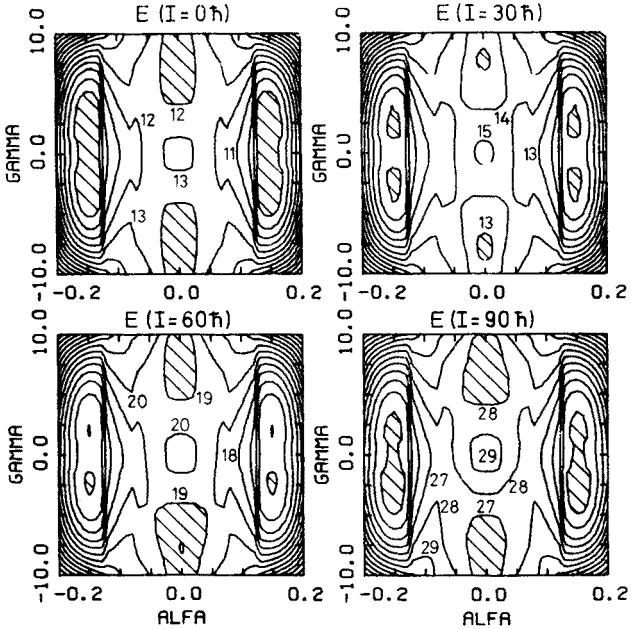

Fig. 9. Deformation energy surfaces of ^{238}U at $\beta = 0.9$, $r = 0.9$ are shown in the plane of the reflection asymmetry parameter α and the nonaxial deformation γ for $I = 0$, 30, 60 and 90$\hbar$. The equienergy lines are drawn in steps of 1 MeV

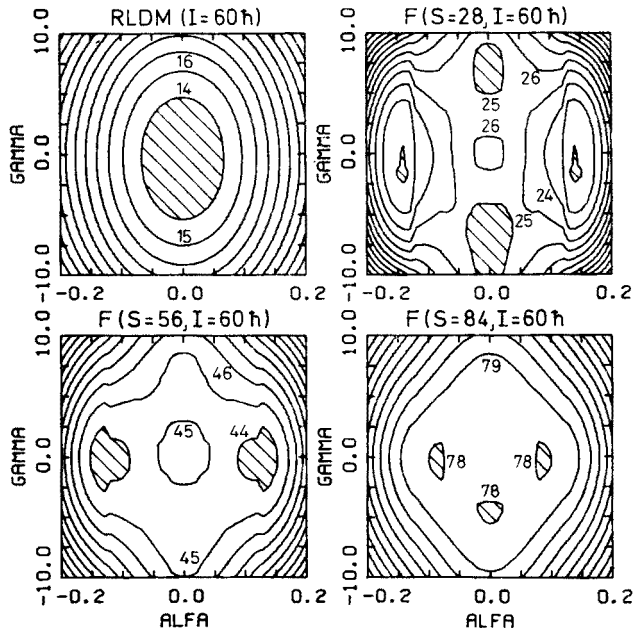

Fig. 10. Energy surfaces of ^{238}U at $I = 60\hbar$ ($\beta = 0.9$, $r = 0.9$) are plotted as a function of the deformation parameters α and γ. The left upper map shows the rotating liquid drop energy surface. The right upper and the lower two maps present the isentropic energy surfaces at $S = 28$, 56 and 84 corresponding to average temperatures of 0.5, 1 and 1.5 MeV. The equienergy lines are drawn in steps of 1 MeV

at the fission barrier of Ra-isotopes was given by Weber et al. [16] who observed that symmetric and asymmetric fission are associated with different thresholds. Similar properties of the fission process were found also in Ac [28] and U [17] isotopes.

The fission mass yields of ^{238}U at various thermal excitations and at $I \sim 0$ were studied by Colby et al. [29]. A sizeable asymmetry in the mass yields was found but no clear maximum was observed for symmetric fission. Figs. 9 and 10 exhibit results of calculations for ^{238}U at the second barrier. Fig. 9 shows the energy surface in the $\alpha-\gamma$-plane at constant deformation parameters β and r ($\beta = 0.9$, $r = 0.9$) which correspond approximately to the fission saddle point at $I = 0$. The energy surfaces in Fig. 10 were calculated at $T = 0$ and for angular momenta $I = 0$, 30, 60 and 90 $\hbar$. At $I = 0$ one can see the double degenerate ($\pm\alpha$) mass asymmetric minimum, a hill at $\alpha = \gamma = 0$ and a small minimum at $\alpha = 0$, $\gamma \sim \pm 7\,5°$. With increasing spin negative γ-deformations become favored.

The results for various models applied to the calculation of DES's in the α, γ-plane ($\beta = 0.9$, $r = 0.9$) at $I = 90\,\hbar$ are shown in Fig. 10. The RLDM surface in the upper left diagram shows a slight tendency towards negative γ-values but is symmetric around $\alpha = 0$. It is known that the reflection asymmetry of nuclear shapes at the second barrier is due to the shell effects. The other three contour plots in Fig. 10 show the energy surfaces at $S = 28$ ($\leftrightarrow \overline{T} = 0.5$ MeV), $S = 56$ ($\leftrightarrow \overline{T} = 1$ MeV) and $S = 84$ ($\leftrightarrow \overline{T} = 1.5$ MeV). The increase in entropy leads to a rapid decrease of the energy difference between the mass asymmetric and the mass symmetric minima from ~ 5 MeV at $S = 0$ to ~ 1 MeV at $S = 56$. Also the reflection asymmetric minimum becomes more shallow corresponding to a broader width of the peaks in the fission fragment mass spectrum. A similar T-dependence of the full width half maximum (FWHM) has been reported e.g. by Colby et al. [29] in ^{238}U. At $S = 84$ ($E^* \sim 80$ MeV) the separate mass asymmetric channel practically disappears and one can see that the fission saddle is very flat in the α, γ-plane. The shell effects which are still present at $\alpha \neq 0$ and $S = 84$ leads to a significant increase of the shallow region of the α, γ-plane as compared with the RLDM results.

In conclusion, the influence of thermal excitations on the mass spectrum of fission products can be discussed in three distinct regions. At low temperatures ($T \lesssim 0.5$ to 1.0 MeV) one observes a sharp increase of the ratio of symmetric P_f(sym) to asymmetric P_f(asym) fission. The FWHM for symmetric and asymmetric fission becomes larger. In the second region (1.0 MeV $\lesssim T \lesssim$ 2.0 MeV) the amplitude of the shell corrections of the reflection asymmetric configurations is comparable with the variations of the classical energy when going from $\alpha = 0$ to α_{min} at the minimum of δE_{sh}. In this temperature region the FWHM approaches a maximum:

$$\Delta_{max} \simeq M_H - M_L + \Delta_{g.s.} \tag{4.1}$$

where M_H, M_L denote the average mass numbers in the group of heavy and light fission fragments respectively and $\Delta_{g.s.}$ is the FWHM value at $I = 0$. Finally at $T \geqslant 2$ MeV the FWHM decreases slowly and tends to a limit which is determined by the curvature of the classical free energy surface in the $\alpha-\gamma$ ($\beta-r$) space.

5. Summary

In this paper we have proposed a new model for the investigation of rotating heated nuclei. This model is based on the Strutinsky shell correction method for finite I and T, but is essentially free from such shortcomings as the spurious contribution of the smoothed density of s.p. states $\tilde{g}(\varepsilon)$ to the nuclear excitation energy at large deformations or the inaccuracies in the classical free energy. The essence of this model is a renormalization of $\tilde{g}(\varepsilon)$ by a LDM-density $g_{\mathrm{LDM}}(\varepsilon)$. The resulting function $g_{\mathrm{R}}(\varepsilon)$ is essentially independent of the thermal energy for $T \lesssim 5$ MeV and, for the SW average potential, it is basically not modified by a rotation. Therefore, the theoretical model described in this work provides a systematic tool for studies of highly excited nuclei and allows to check assumptions made for $g_{\mathrm{LDM}}(\varepsilon)$ by a detailed comparison with the experimental data in various regions of mass and excitation energies.

We have compared the properties of the heated, rotating nuclei ^{210}Po and ^{238}U in the isothermal and isentropic limits. Nuclear properties around the fission saddle point can be discussed in three regions of thermal excitations. The first region ($T \lesssim 1$ MeV) is characterized by relatively strong shell effects which determine the shape changes, fission stability and decay properties of nuclei. For isentropic processes one observes in this region a large decrease of the temperature variations with deformation and a large increase in the ratio $P_f(\mathrm{sym})/P_f(\mathrm{asym})$. In the second region of temperature ($1 \lesssim T \lesssim 1.5$ MeV), variations of δE_{sh} as a function of deformation are comparable with corresponding changes of E_{RLDM}. Thus, one finds that the FWHM approaches a maximum and symmetric fission becomes dominant ($P_f(\mathrm{sym}) > P_f(\mathrm{asym})$). Moreover, the stiffness of the equilibrium shape shows a sharp minimum at the angular momenta close to I_{CRIT}. In the third region of temperatures ($1.5 \lesssim T \lesssim 2$ MeV) the classical part of the energy is decisive and determines the properties of highly excited nuclei. Thus, the asymmetric component in the fission fragment mass distribution disappears and the FWHM approaches the limit governed by the RLDM.

The calculations of properties of heated, rotating nuclei indicate several characteristic features which result from shell effects at finite I and T and could be studied experimentally. Among the most promising experiments are the detailed measurements of the competition between fission and particle emission (n, p, α) at very high spins and at relatively low temperatures ($T \lesssim 1.5$ MeV). Such data will give information on the nuclear stability and shape changes for spins close to the limiting angular momenta for the stability of compound nuclei.

REFERENCES

[1] M. Ploszajczak, M. Faber, *Phys. Rev. Lett.* **43**, 498 (1979); M. Ploszajczak, M. Faber, *Phys. Rev.* **C25**, 1538 (1982).

[2] A. Faessler, K. R. Sandhya Devi, F. Grümmer, K. W. Schmid, R. R. Hilton, *Nucl. Phys.* **A256**, 106 (1976); M. Ploszajczak, K. R. Sandhya Devi, A. Faessler, *Z. Physik* **A282**, 267 (1977).

[3] C. G. Andersson, S. E. Larsson, G. Leander, P. Möller, S. G. Nilsson, I. Ragnarsson, S. Åberg, R. Bengtsson, J. Dudek, B. Nerlo-Pomorska, K. Pomorski, Z. Szymański, *Nucl. Phys.* **A268**, 205 (1976).

[4] K. Neergård, V. V. Pashkevich, S. Frauendorf, *Nucl. Phys.* **A262**, 61 (1976).
[5] K. Neergård, H. Toki, M. Ploszajczak, A. Faessler, *Nucl. Phys.* **A287**, 48 (1977).
[6] M. Ploszajczak, H. Toki, A. Faessler, *Z. Physik* **A287**, 103 (1978); T. Døssing, K. Neergård, K. Matsuyanagi, Hsi-Chen-Chang, *Phys. Rev. Lett.* **39**, 1395 (1977).
[7] M. Faber, M. Ploszajczak, A. Faessler, *Nucl. Phys.* **A326**, 129 (1979).
[8] S. Cohen, F. Plasil, W. J. Swiatecki, *Ann. Phys.* **82**, 557 (1974).
[9] A. V. Ignatiuk, I. N. Mikhailov, R. G. Nazmitdinov, B. Nerlo-Pomorska, K. Pomorski, *Phys Lett.* **76B**, 543 (1978).
[10] M. E. Faber, M. Ploszajczak, *Z. Physik* **A291**, 331 (1979).
[11] M. Hillman, *Phys. Rev.* **C7**, 2037 (1973).
[12] P. A. Gottschalk, T. Ledergerber, *Nucl. Phys.* **A278**, 16 (1977).
[13] M. Diebel, K. Albrecht, R. W. Hasse, *Nucl. Phys.* **A355**, 66 (1981).
[14] R. W. Hasse, W. Stocker, *Phys. Lett.* **44B**, 26 (1973).
[15] W. Stocker, J. Burzlaff, *Nucl. Phys.* **A202**, 265 (1973).
[16] J. Weber, H. C. Britt, A. Gavron, E. Konecny, J. B. Wilhelmy, *Phys. Rev.* **C13**, 2413 (1976).
[17] A. Gavron, H. C. Britt, P. D. Goldstone, J. B. Wilhelmy, S. E. Larsson, *Phys. Rev. Lett.* **38**, 1457 (1977); K. Junker, J. Hadermann, *Z. Physik* **A282**, 391 (1977); K. Junker, EIR-Bericht 292 (1976).
[18] H. C. Pauli, *Phys. Rep.* **7**, 35 (1973).
[19] S. Cohen, W. J. Swiatecki, *Ann. Phys.* **19**, 67 (1972).
[20] A. Bohr, *K. Dan. Vidensk. Selsk. Mat. Fys. Medd.* **26**, Nov. 14 (1952).
[21] G. Sauer, H. Chandra, U. Mosel, *Nucl. Phys.* **A264**, 221 (1976).
[22] G. Süssmann, *Z. Physik* **274**, 145 (1975).
[23] A. V. Ignatyuk, I. N. Mikhailov, L. H. Molina, R. G. Nazmitdinov, P. Pomorski, *Nucl. Phys.* **A346**, 191 (1980).
[24] R. Balian, C. Bloch, *Ann. Phys.* **60**, 401 (1970); **64**, 271 (1971); **69**, 76 (1972).
[25] W. D. Myers, *Nucl. Phys.* **A145**, 387 (1970).
[26] R. C. Jensen, A. W. Fairhall, *Phys. Rev.* **109**, 942 (1958).
[27] E. Konecny, H. W. Schmitt, *Phys. Rev.* **172**, 1226 (1968).
[28] E. Konecny, H. J. Specht, J. Weber, *Phys. Lett.* **45B**, 329 (1973) and in Proc. Third Conf. on the Physics and Chemistry of Fission, Rochester 1973, Vol. 2, IAEA, Vienna 1974, p. 3.
[29] L. J. Colby, Jr., M. L. Shoaf, J. W. Cobble, *Phys. Rev.* **121**, 1415 (1961).
[30] M. Brack, J. Damgaard, A. S. Jensen, H. C. Pauli, V. M. Strutinsky, C. Y. Wong, *Rev. Mod. Phys.* **44**, 320 (1972).